



Showcasing research from Professor Jintong Song's laboratory, College of Chemistry and Materials Science, Sichuan Normal University, and Professor Haifeng Xiang's laboratory, College of Chemistry, Sichuan University, Chengdu, China.

Building metal-induced inherent chirality: chiral stability/phosphorescence enhancement *via* a ring expansion strategy of Pt(II) complexes

In the present work, inherently chiral (cR)/(cS)Pt(II) complexes with 3D boat form were designed and prepared by using achiral ligands for highly chiral stability and phosphorescence quantum yield (up to 81.0%).

Image reproduced by permission of Jintong Song and Haifeng Xiang from *Chem. Sci.*, 2025, **16**, 9135.

As featured in:



See Haifeng Xiang,
Jintong Song *et al.*,
Chem. Sci., 2025, **16**, 9135.

Cite this: *Chem. Sci.*, 2025, **16**, 9135

All publication charges for this article have been paid for by the Royal Society of Chemistry

Received 12th February 2025

Accepted 25th April 2025

DOI: 10.1039/d5sc01121c

rsc.li/chemical-science

Building metal-induced inherent chirality: chiral stability/phosphorescence enhancement *via* a ring expansion strategy of Pt(II) complexes†

Yingshuang Shi,^a Ke Tang,^a Jincheng Zhang,^a Ping Hu,^a Bi-Qin Wang,^a Ke-Qing Zhao,^a Yuqiao Zhou,^a Haifeng Xiang^b and Jintong Song^{a*}

Chirality is indeed a fundamental aspect of nature, particularly in chemistry and biology. Herein, we have demonstrated a straightforward strategy to create a novel type of metal-induced inherent chirality by expanding coordination rings. Typically, tetracoordinated d⁸ Pt(II) complexes with two five-membered coordination rings are 2D square-planar, resulting in the absence of chirality. However, if one of the coordination rings is expanded to six or seven members, the molecular structures of Pt(II) complexes would transition from a 2D plane to a 3D boat-like configuration. This not only facilitates the construction of inherently chiral scaffolds but also addresses the problem of emission aggregation-caused quenching. Furthermore, the strategy of ring expansion can enhance the chiral stability and phosphorescence quantum yield (up to 81.0%). Thus, the present work introduces a new structural motif with promising potential for application as chiroptical and luminescent materials.

Introduction

Chirality, referring to molecules that cannot fully overlap with their mirror images, is a fundamental property present in nature,¹ and thus the development of novel chiral molecules plays a pivotal role in biochemistry, asymmetric synthesis,² supramolecular chemistry,³ chiral optics,⁴ and so on. In general, chirality of organic molecules can be classified into four categories: point, axial, helical, and planar.⁵ The term “inherently chiral” was first suggested by Böhmer for chiral calixarenes, which do not strictly fall into definitions of other types of chirality.⁶ Later, a more general definition was formulated in 2004 by the group of Mandolini and Schiaffino.⁷ It states that inherent chirality derives from the “introduction of a curvature in an ideal planar structure that is devoid of symmetry axes in its bidimensional representation”.⁸ Since then, the concept of inherent chirality has been increasingly used to denote chirality arising from the rigid structures in both medium-sized rings (no less than a seven-membered ring)⁹ and large-sized rings (such as rotaxanes, catenanes, fullerenes, cavitands, and capsular assemblies).¹⁰ However, these pure organic molecules usually exhibit fluorescence.^{9a,11}

Cyclometalated Pt(II) complexes have been extensively investigated in the past two decades owing to their rich phosphorescence properties and wide applications in phosphorescent organic light emitting diodes,¹² chemosensors,¹³ bio-imaging,¹⁴ circularly polarized luminescence (CPL),^{5a,d,15} and so on. Typically, tetracoordinated d⁸ Pt(II) complexes with two five-membered coordination rings are 2D square-planar,¹⁶ resulting in the lack of chirality. Moreover, these square-planar molecules are far more likely to encounter the problem of emission “aggregation-caused quenching” (ACQ), because they readily form dimers through not only intermolecular π-π stacking interactions but also Pt^{II}-Pt^{II} interactions.¹⁴ Therefore, the chirality of Pt(II) complexes is primarily introduced by chiral ligands.^{5d,15,17} Although there are limited examples of chiral Pt(II) complexes with achiral ligands,¹⁸ their chiroptical properties, especially CPL, have seldom been reported before, mainly due to not only the weak chirality but also low phosphorescence quantum yields (Φ). Herein, we have demonstrated a straightforward strategy to build a novel type of metal-induced inherent chirality by expanding coordination rings (Fig. 1). When using N1^{AO}, N2^{AO}, N^{AP}, N^{APS}, and N^{PO} bidentate ligands, one of the coordination rings expands into six or seven members. The molecular structures of Pt(II) complexes would change from 2D plane into 3D boat-like configuration, which not only facilitates the construction of inherently chiral scaffolds but also resolves the ACQ problem. Moreover, the strategy of ring expansion can improve the chiral stability and phosphorescence quantum yield (up to 81.0%). Furthermore, the resultant enantiomers of complexes can be separated by chiral high-performance liquid chromatography (HPLC), and their

^aCollege of Chemistry and Materials Science, Sichuan Normal University, Chengdu 610066, China. E-mail: jintongsong@sicnu.edu.cn

^bCollege of Chemistry, Sichuan University, Chengdu 610065, China. E-mail: xianghaifeng@scu.edu.cn

† Electronic supplementary information (ESI) available. CCDC 2378928–2378930, 2378935, 2378936, 2378939 and 2386027. For ESI and crystallographic data in CIF or other electronic format see DOI: <https://doi.org/10.1039/d5sc01121c>



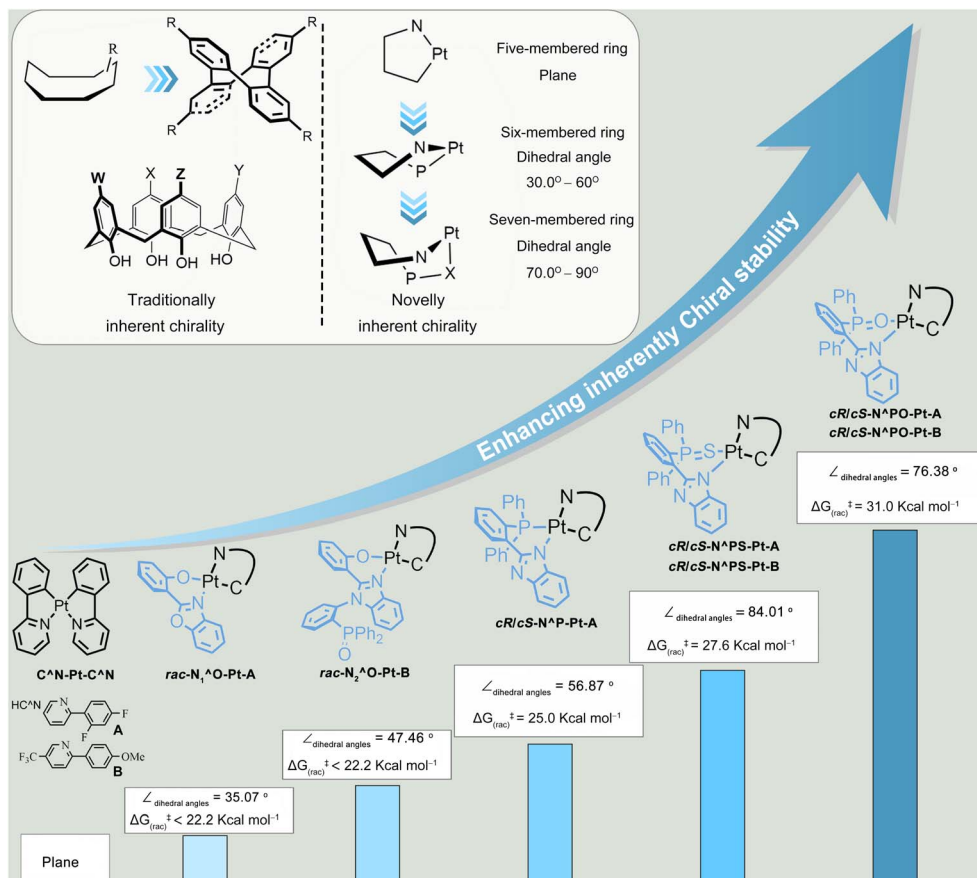


Fig. 1 The designed scheme and chemical structures of inherently chiral Pt(II) complexes (\angle dihedral angles: angle between the phenyl plane and the PtC²⁺N coordination plane; $\Delta G_{(rac)}^{\ddagger}$: racemization energy barriers of inherently chiral Pt(II) complexes).

absolute configuration is confirmed by X-ray diffraction, circular dichroism, CPL, and density functional theory calculation.

Results and discussion

Synthesis and characterization

The synthetic methods for the ligands and Pt(II) complexes are detailed in the ESI.† Initially, we utilized N1¹O, N2¹O, and N¹P ligands to synthesize the Pt(II) complexes with six-membered coordination rings. N¹PS and N¹PO ligands were used to prepare the Pt(II) complexes with seven-membered coordination rings. Single crystals of **rac-N1¹O-Pt-A** (CCDC: 2378928), **rac-N2¹O-Pt-B** (CCDC: 2378929), **rac-N¹P-Pt-A** (CCDC: 2378930), **rac-N¹PS-Pt-A** (CCDC: 2378935), **rac-N¹PO-Pt-A** (CCDC: 2378936), **rac-N¹PS-Pt-B** (CCDC: 2378939), and **rac-N¹PO-Pt-B** (CCDC: 2386027) were obtained through slow diffusion and evaporation of a hexane/CH₂Cl₂ solution.

First, chiral HPLC was used to analyze and separate enantiomers of the Pt(II) complexes. For **rac-N1¹O-Pt-A** and **rac-N2¹O-Pt-B** (Fig. S1†), there exists only one chromatographic peak in the HPLC trace. The possible reason is that the steric hindrance of N1¹O and N2¹O is too small to stabilize chirality in solution. With strong steric hindrance from two phenyl

groups in triphenyl phosphine, **rac-N¹P-Pt-A**, **rac-N¹PS-Pt-A**, **rac-N¹PO-Pt-A**, **rac-N¹PS-Pt-B**, and **rac-N¹PO-Pt-B** have two separated chromatographic peaks featuring a 1 : 1 ratio of the area (Fig. 2). The first peak (black line) refers to the optically pure **cR-N¹P-Pt-A**, **cR-N¹PS-Pt-A**, **cR-N¹PO-Pt-A**, **cR-N¹PS-Pt-B**, and **cR-N¹PO-Pt-B**, while the second one (red line) corresponds to the **cS-N¹P-Pt-A**, **cS-N¹PS-Pt-A**, **cS-N¹PO-Pt-A**, **cS-N¹PS-Pt-B**, and **cS-N¹PO-Pt-B** (see the later discussion). Enantiopure **cR** and **cS**-Pt(II) complexes (>98% ee) were collected by chiral HPLC, albeit the recovered yield being inferior to 30%.

Photophysical properties and calculations

Table 1 presents the UV/visible absorption and emission data of Pt(II) complexes at room temperature. As illustrated in Fig. 3, **rac-N1¹O-Pt-A**, **rac-N¹P-Pt-A**, **rac-N¹PO-Pt-A**, and **rac-N¹PS-Pt-A** with a common HC²⁺N ligand of 2-(4',6'-difluorophenyl)pyridine (**A**) exhibit low-energy absorption bands at λ_{abs} = 402, 380, 375, and 358 nm, respectively, demonstrating a gradual blue shift. This trend contrasts with the trend of corresponding dihedral angles, which are 35.07°, 56.87°, 76.38°, and 84.01° for **rac-N1¹O-Pt-A**, **rac-N¹P-Pt-A**, **rac-N¹PO-Pt-A**, and **rac-N¹PS-Pt-A**, respectively. A bigger dihedral angle would lead to a smaller degree of conjugation and a blue-shifted absorption band consequently (see the later discussion). **rac-N¹PO-Pt-A** and **rac-**

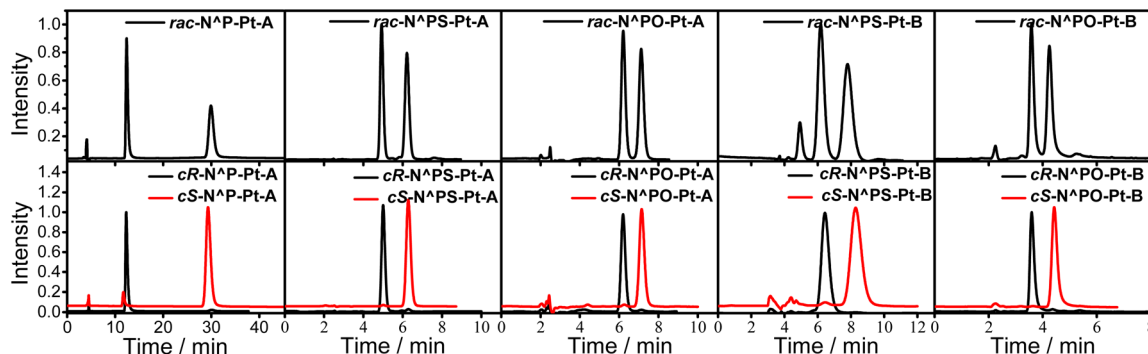


Fig. 2 Top: chiral HPLC traces of **rac-N^P-Pt-A**, **rac-N^{PS}-Pt-A**, **rac-N^{PO}-Pt-A**, **rac-N^{PS}-Pt-B**, and **rac-N^{PO}-Pt-B**. Bottom: chiral HPLC traces of enantiopure (*cR*) (black line) and (*cS*) (red line) Pt(II) complexes.

N^{PO}-Pt-B with the same **N^{PO}** but different **C^N** ligands display low-energy absorption bands at $\lambda_{\text{abs}} = 375$ and 419 nm, respectively. All the above results indicate that not only **N1^O, N2^O, N^P, N^{PS}, and N^{PO} but also **HC^N** ligands have an obvious impact on absorption spectra.**

Density functional theory (DFT) and time-dependent DFT (TD-DFT) calculations were conducted using the Gaussian 09 program package to investigate the mechanisms of excited states and transitions. In dilute CH_2Cl_2 solution, both the absorption spectral bands and molar absorption coefficients (ϵ) of Pt(II) complexes are well-replicated by theoretical computations (Fig. 3 and S2–S4†). The low-energy absorption bands of **rac-N^{PS}-Pt-A**, **rac-N^{PO}-Pt-A**, and **rac-N^P-Pt-A** are 358 nm, 375 nm, and 380 nm, respectively, which are accurately reproduced by TD-DFT calculations (calculated $\lambda_{\text{abs}} = 362$ nm, 365 nm, and 388 nm for **cS-N^{PS}-Pt-A**, **cS-N^{PO}-Pt-A**, and **cS-N^P-Pt-A**, respectively). These low-energy absorption bands are primarily attributed to the transition from the highest occupied molecular orbital (HOMO) to the lowest unoccupied molecular orbital (LUMO) with contributions exceeding 80%, and the corresponding oscillator strength (f_{osc}) values are 0.0075, 0.0288, and 0.0389 for **cS-N^{PS}-Pt-A**, **cS-N^{PO}-Pt-A**, and **cS-N^P-Pt-A**, respectively. The energy level diagram and frontier molecular orbitals indicate that the electron cloud of the HOMO is predominantly contributed by the electron-rich Pt(II) ions and

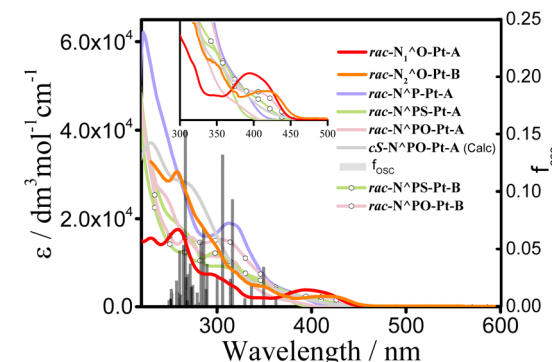


Fig. 3 Experimental absorption spectra of Pt(II) complexes in CH_2Cl_2 solution (5.0×10^{-5} mol dm^{-3}).

the **1H**-benzo[*d*]imidazole segments of the **N^P**, **N^{PS}**, and **N^{PO}** ligands, while the LUMO's electron cloud is mainly derived from the electron-deficient **HC^N** ligands (Fig. 4). Consequently, the low-energy absorption bands are primarily attributed to metal-to-ligand charge transfer (MLCT) from Pt(II) ions to **C^N** ligands, as well as ligand-to-ligand charge transfer (LLCT) from **1H**-benzo[*d*]imidazole to **HC^N** ligands. Not only **N^P**, **N^{PS}**, and **N^{PO}** ligands but also **HC^N** ligands have obvious contributions to low-energy absorption bands, which is in accord with UV-visible absorption data (Table 1).

Table 1 Room-temperature photophysical properties of binuclear Pt(II) complexes

Compounds	Medium	$\lambda_{\text{abs}}/\text{nm}$ ($\epsilon/\text{dm}^3 \text{ mol}^{-1} \text{ cm}^{-3}$)	$\lambda_{\text{em}}/\text{nm}$	Φ_{PL}	$\tau_{\text{p}}/\mu\text{s}$
rac-N^P-Pt-A	CH_2Cl_2	$316 (1.84 \times 10^4)$, $380 (2.99 \times 10^3)$	—	—	—
	Powder	—	$468/496/535$	0.45%	1.11
rac-N^{PS}-Pt-A	CH_2Cl_2	$267 (1.68 \times 10^4)$, $318 (9.01 \times 10^3)$, $358 (4.25 \times 10^3)$	—	—	—
	Powder	—	$466/500/535$	6.61%	0.97
rac-N^{PO}-Pt-A	CH_2Cl_2	$247 (2.47 \times 10^4)$, $317 (1.02 \times 10^4)$, $375 (1.60 \times 10^3)$	—	—	—
	Powder	—	$473/502/544$	29.4%	0.94
rac-N^{PS}-Pt-B	CH_2Cl_2	$296 (1.22 \times 10^4)$, $410 (1.43 \times 10^3)$	—	—	—
	Powder	—	$506/538$	3.39%	8.51
rac-N^{PO}-Pt-B	CH_2Cl_2	$311 (1.48 \times 10^4)$, $419 (1.89 \times 10^3)$	—	—	—
	Powder	—	$521/549$	81.0%	9.27



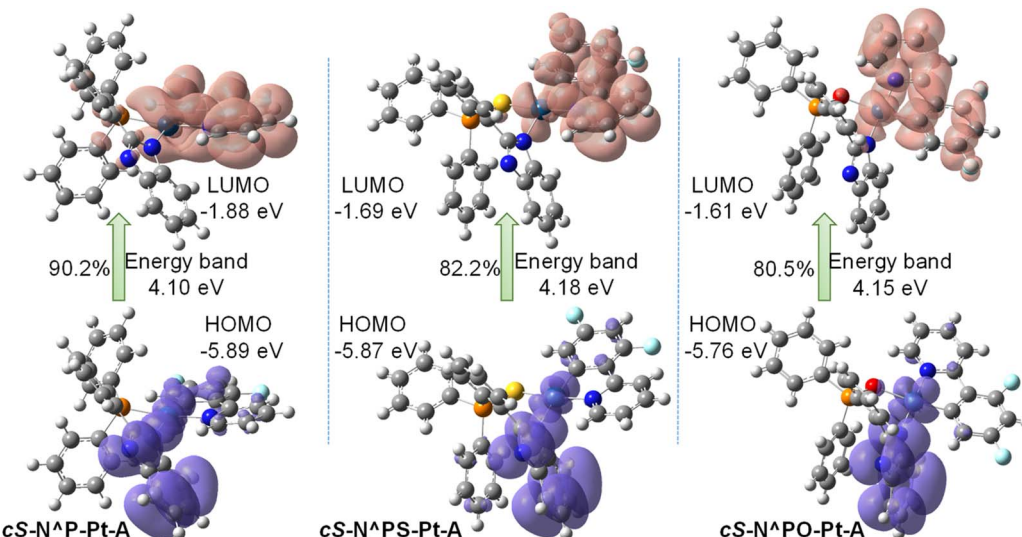


Fig. 4 Energy level diagram and frontier molecular orbitals of **cS-N^{^P}-Pt-A**, **cS-N^{^PS}-Pt-A**, and **cS-N^{^PO}-Pt-A** (in CH_2Cl_2).

All the Pt(II) complexes are weakly emissive or non-emissive in a dilute degassed CH_2Cl_2 solution. In comparison with solution samples, their powders show significant aggregation-induced emission (AIE)¹⁹ with promising quantum yields (3.76%, 4.40%, 0.45%, 6.61%, 29.4%, 3.39%, and 81.0% for **rac-N1^{^O}-Pt-A**, **rac-N2^{^O}-Pt-B**, **rac-N^{^P}-Pt-A**, **rac-N^{^PS}-Pt-A**, **rac-N^{^PO}-Pt-A**, **rac-N^{^PS}-Pt-B**, and **rac-N^{^PO}-Pt-B**, respectively) (Fig. 5, S5, Tables 1 and S1†). Based on their relatively long emission decay lifetimes in the microsecond range (μs , Fig. S6, S7,† and Table 1) and significant Stokes shifts (ranging from 140 nm to 170 nm) between the absorption and emission bands, the emission from Pt(II) complexes can be classified as phosphorescence, originating from triplet excited states. As illustrated in Fig S8,† the frontier molecular orbitals in the triplet excited states of Pt(II) complexes (in CH_2Cl_2 solution) are analogous to those in singlet excited states, suggesting that their phosphorescence predominantly arises from $^3\text{MLCT}$ and $^3\text{LLCT}$.

X-ray single-crystal structures

The molecular structure and packing in X-ray single crystals of **rac-N^{^PS}-Pt-A** and **rac-N^{^PO}-Pt-A** are illustrated in Fig. 6. Unlike the traditional inherently chiral molecules, according to the definition of calixarenes, curvature is denoted as ‘c’, with clockwise as ‘cR’ and counterclockwise as ‘cS’.^{12,13} The core skeletons of these Pt(II) complexes are chiral (Fig. 1), and such metal-induced chirality can also be defined as inherent chirality for simplicity. An ideal observer standing on the cabin (the concave side of the surface) will see a seven-membered ring (Pt, O, P, C, C, C, and N atoms) at the side of the boat. The clockwise or counterclockwise array of the three highest priority atoms is designated as (cR) or (cS), respectively, as shown in Fig. 6. As anticipated, there are a pair of (cR)/(cS) enantiomers in their single crystals [**cR-N^{^PO}-Pt-A** and **cS-N^{^PO}-Pt-A**; **cR-N^{^PS}-Pt-A** and **cS-N^{^PS}-Pt-A**], corroborating the viability of our design strategy. Additionally, the enantiomers of **rac-N1^{^O}-Pt-A**, **rac-N2^{^O}-Pt-B**, **rac-N^{^PS}-Pt-B**, and **rac-N^{^PO}-Pt-B** (Fig. S9–S11†) are also discernible within the single-crystal structures.

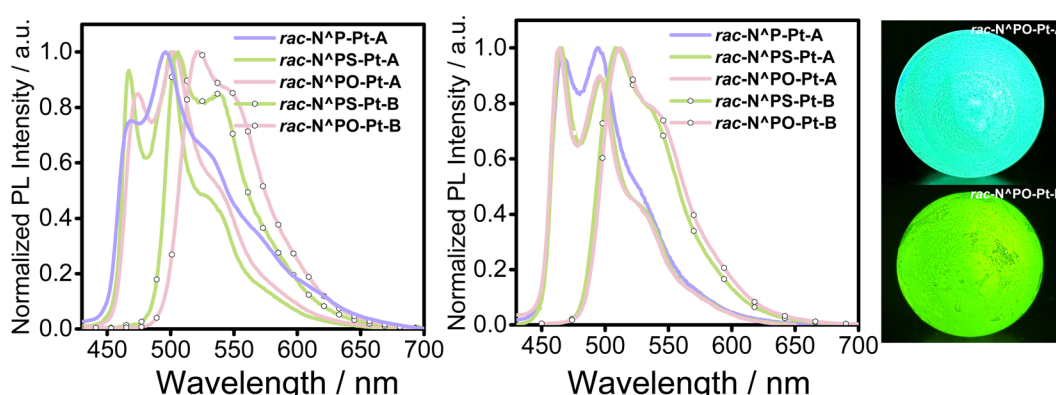


Fig. 5 PL spectra of **rac-N^{^P}-Pt-A**, **rac-N^{^PS}-Pt-A**, **rac-N^{^PO}-Pt-A**, **rac-N^{^PS}-Pt-B**, and **rac-N^{^PO}-Pt-B** in the powder and doped film. Photographs of **rac-N^{^PO}-Pt-A**, and **rac-N^{^PO}-Pt-B** in the powder under a 365 nm UV lamp.

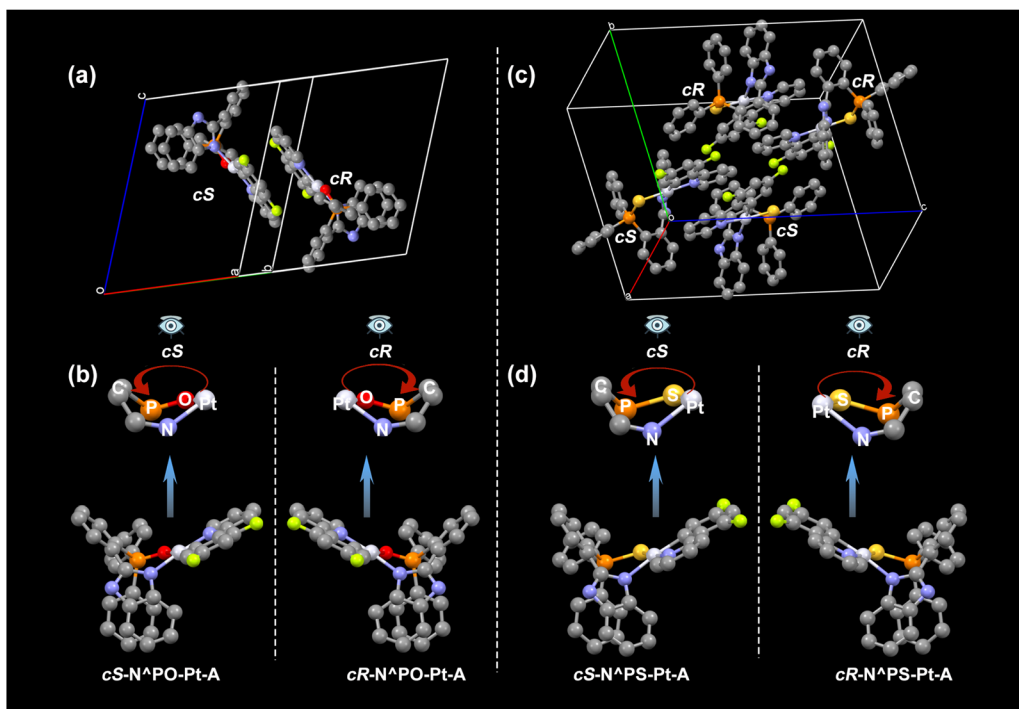


Fig. 6 X-ray single-crystal structures of **rac-N¹^PO-Pt-A**: (a) one crystal cell and (b) **cR-N¹^PO-Pt-A** and **cS-N¹^PO-Pt-A** molecular structures and the definition of (cR)/(cS) chirality (some atoms are omitted); X-ray single-crystal structures of **rac-N¹^PS-Pt-A**: (c) one crystal cell and (d) **cR-N¹^PS-Pt-A** and **cS-N¹^PS-Pt-A** molecular structures and the definition of (cR)/(cS) chirality (some atoms are omitted).

The photoluminescence properties of Pt(II) complexes are significantly influenced by their molecular structures and arrangements. There are no freely rotating groups for **rac-N1¹O-Pt-A**, and **rac-N2²O-Pt-B**; however, their solutions are weakly emissive. This suggests the molecular backbone vibration to promote the non-radiative decay process.^{11,20} The other Pt(II) complexes contain not only molecular backbone vibration but also C-P-bond-linked phenyl groups, which are capable of free motion and consequently offer a possible pathway for the non-radiative annihilation of their excited states in solution. On the other hand, there are many strong intermolecular interactions, such as F-H (2.627–2.933 Å), C-H (2.665–2.886 Å), N-H (2.551–2.862 Å), O-H (2.410–2.713 Å), and H-H (2.350–2.769 Å) interactions (Fig. S9–S12†) in the single crystals of **rac-N¹P-Pt-A**, **rac-N¹PS-Pt-A**, **rac-N¹PO-Pt-A**, **rac-N¹PS-Pt-B**, and **rac-N¹PO-Pt-B**. These strong intermolecular interactions can inhibit the rotation of C-P single bonds. The metal–metal interactions can significantly alter the photophysical properties of the complexes, such as red-shifted spectra and changes in the nature of the charge transfer transitions.²¹ Moreover, these resultant Pt(II) complexes adopt a 3D boat-like structure, which hinders intermolecular face-to-face π - π stacking interaction and intermolecular Pt^{II}–Pt^{II} interactions (5.871–8.033 Å, Fig. S10–S12†) between adjacent complexes. Under the above synergistic effects, these Pt(II) complexes exhibit a substantial AIE phenomenon¹⁹ (0.45%, 6.61%, 29.4%, 3.39%, and 81.0% for **rac-N¹P-Pt-A**, **rac-N¹PS-Pt-A**, **rac-N¹PO-Pt-A**, **rac-N¹PS-Pt-B**, and **rac-N¹PO-Pt-B**, respectively).

In theory, the emission quantum yield of a square-planar Pt(II) complex is strongly dependent on the planeness of coordination. The lesser the torsion is, the higher the quantum yield. For all the AIE-active Pt(II) complexes, the Pt atoms and **HC¹N** ligands are nearly coplanar. However, their emission quantum yields are quite different. The torsion angle of C1–C2–Pt–P, C1–C2–Pt–S, C1–N1–Pt–O, C1–C2–Pt–S, and C1–N1–Pt–O is 16.99°, 1.68°, 1.01°, 3.87°, and 3.01° for **cS-N¹P-Pt-A**, **cS-N¹PS-Pt-A**, **cS-N¹PO-Pt-A**, **(cS)N¹PS-Pt-B**, and **cS-N¹PO-Pt-B**, respectively. Additionally, the torsion angle of C3–N1–Pt–N2, C3–N1–Pt–N2, C2–C3–Pt–N2, C3–N1–Pt–N2, and C2–C3–Pt–N2 is 15.54°, 9.66°, 7.53°, 9.60°, and 4.42° for **(cS)N¹P-Pt-A**, **cS-N¹PS-Pt-A**, **cS-N¹PO-Pt-A**, **cS-N¹PS-Pt-B**, and **cS-N¹PO-Pt-B**, respectively. **cS-N¹PO-Pt-A**, and **cS-N¹PO-Pt-B** have a less distorted square-planar geometry, resulting in their high emission quantum yields (Fig. 7).

Racemization experiment

The chirality of these Pt(II) complexes originated from their 3D boat-type structures. If the cocked phenyl group in **N1¹O**, **N2²O**, **N¹P**, **N¹PS**, and **N¹PO** ligands flips down into the coplane with the coordination system, racemization would occur. Therefore, the chiral stability is determined by the dihedral angle between the phenyl group and the coordination system. The dihedral angles of these Pt(II) complexes exhibit a positive correlation with both the size of the ring and the peripheral substituent groups. It is reported that enantiomers with racemization energy barriers more than 22.2 kcal mol⁻¹ could be separable at



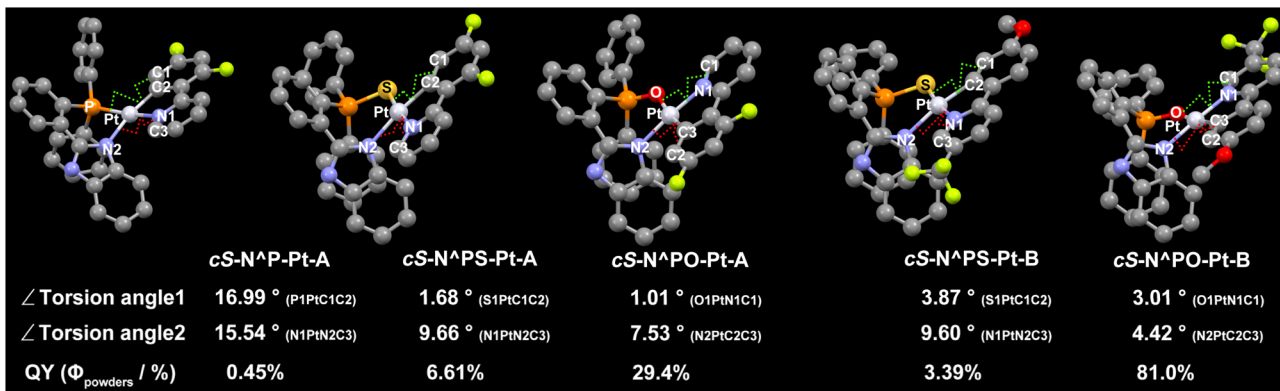


Fig. 7 The relationship between emission quantum yields and torsion angles of coordinated atoms among the representative products: cS-N^P-Pt-A, cS-N^{PS}-Pt-A, cS-N^{PO}-Pt-A, cS-N^{PS}-Pt-B, and cS-N^{PO}-Pt-B.

room temperature.²² The chirality of **rac**-N¹O-Pt-A and **rac**-N²O-Pt-B is not stable in solution, because they don't have a large steric group of triphenyl phosphine. The chirality of other Pt(II) complexes with a triphenyl phosphine group is stable and separable. The dihedral angle of cS-N¹O-Pt-A, cS-N²O-Pt-B, cS-N^P-Pt-A, cS-N^{PO}-Pt-A, and cS-N^{PS}-Pt-A is measured to be 35.07°, 47.46°, 56.87°, 76.38°, and 84.01°, respectively (Fig. 8a). Following Curran's methodology,²³ the fitting of cS-N^P-Pt-A, cS-N^{PO}-Pt-A, and cS-N^{PS}-Pt-A is to

calculate the flipping energy barrier. The energy barriers calculated by fitting are shown in Fig. 8b, which are 25.0 kcal mol⁻¹ (half life, $t_{1/2} = 1.50$ days at 25 °C), 27.6 kcal mol⁻¹ ($t_{1/2} = 0.31$ years at 25 °C), and 31.0 kcal mol⁻¹ ($t_{1/2} = 94$ years at 25 °C), respectively (Tables S1–S3†). The sulfur atom in the N^{PS} ligands is undoubtedly larger than the oxygen atom in the N^{PO} ligands. Therefore, the increased repulsive force from the sulfur atom results in a more distorted seven-membered ring in cS-N^{PS}-Pt-A compared to cS-N^{PO}-Pt-A, which is evidenced by the

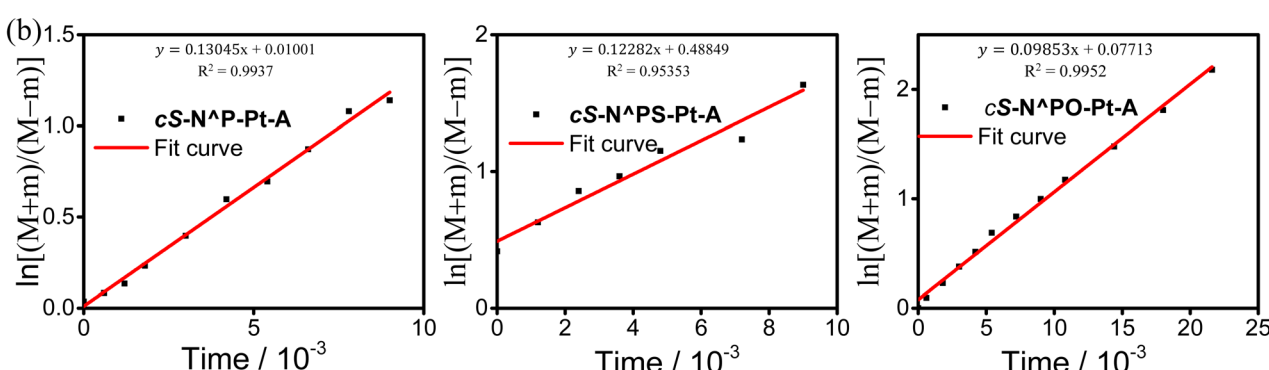
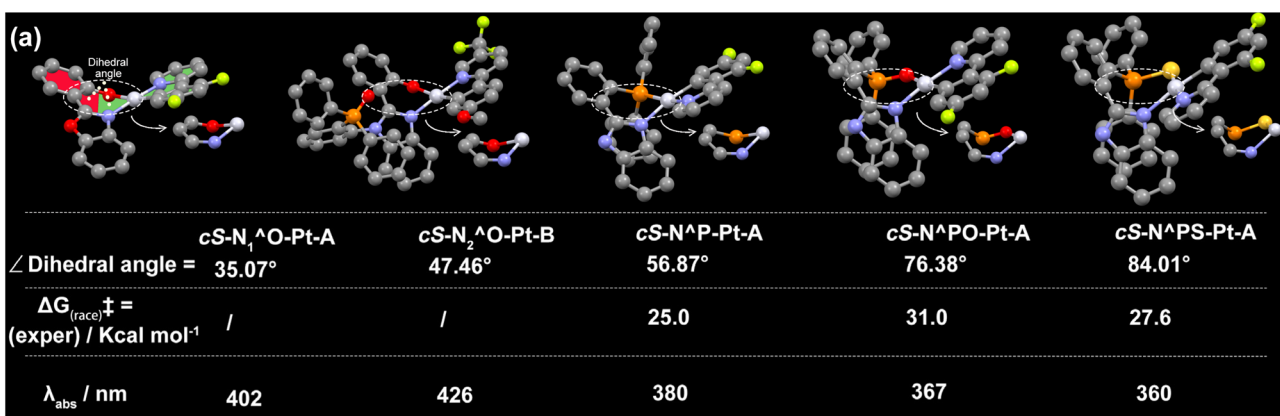


Fig. 8 (a) X-ray single-crystal structures, dihedral angles, and experimental interconversion energy barriers of cS-N¹O-Pt-A, cS-N²O-Pt-B, cS-N^P-Pt-A, cS-N^{PO}-Pt-A, and cS-N^{PS}-Pt-A; (b) investigation of rotation barriers of cS-N^P-Pt-A, cS-N^{PO}-Pt-A, and (cS)N^{PS}-Pt-A.



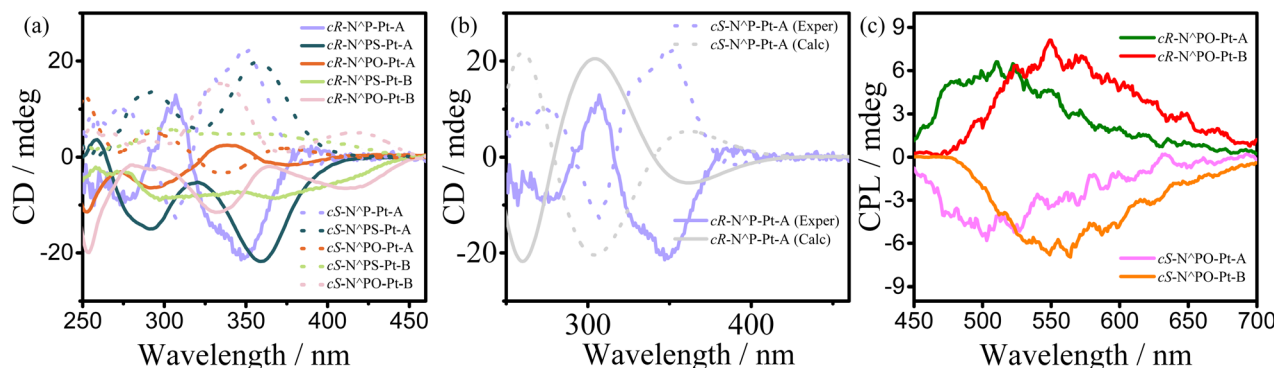


Fig. 9 (a) CD spectra of Pt(II) complexes in dilute CH₂Cl₂ solution (3.0×10^{-5} mol dm⁻³); (b) experimental and calculated CD spectra of cR/cS-N^AP-Pt-A complexes in dilute CH₂Cl₂ solution; (c) CPL spectra of Pt(II) complexes in powder.

larger dihedral angle of cS-N^APS-Pt-A (84.01°) than that of cS-N^APO-Pt-A (76.38°).

Chiroptical properties

The chiroptical properties of Pt(II) complexes were examined using circular dichroism (CD) and CPL spectroscopy (Fig. 9). The CD spectra of the enantiomers in dilute CH₂Cl₂ solution (3.0×10^{-5} mol dm⁻³) exhibit perfect mirror images. The calculated CD spectra closely correspond to the experimental spectra, further confirming the absolute stereochemistry. Analyzing the calculations, the CD peaks in the range of 350–450 nm can be attributed to the MLCT and LLCT. The chirality of square-planar d⁸ Pt(II) complexes is predominantly introduced through the use of chiral ligands, and there are only limited examples of chiral Pt(II) complexes derived from achiral ligands. However, the $|g_{\text{Lum}}|$ of these chiral Pt(II) complexes typically range around 10^{-3} , and they often exhibit low photoluminescence quantum yields (Φ). The CPL spectra of the resulting Pt(II) complexes in the solid state are shown in Fig. 9 and closely correspond to their photoluminescence (PL) spectra. The $|g_{\text{PL}}|$ values at the emission maxima (λ_{em}) are approximately $1.0\text{--}2.0 \times 10^{-3}$, which are comparable to those observed in typical small organic molecules.²⁴ Nevertheless, both the luminescence dissymmetry factors and quantum yields require further enhancement to meet practical application standards. Recent studies have shown that chiral Pt(II) complexes can achieve markedly enhanced g_{Lum} values *via* the construction of chiral supramolecular architectures through intermolecular interactions,^{12g,25} highlighting a compelling strategy for advancing next-generation CPL-active materials.

Conclusions

In this study, we developed a straightforward and efficient strategy to construct a novel type of (cR)/(cS) inherent chirality through metal coordination. These Pt(II) complexes, featuring a boat-type conformation, face challenges related to the absence of metal-induced chirality and the risk of ACQ for square-planar complexes. They exhibit intense blue-green and green phosphorescence with high quantum yields and moderate

asymmetry factors. These findings provide valuable insights into the design of metal-doped chiral materials and their potential applications.

Data availability

The data supporting this article have been included as part of the ESI.† Deposition numbers 2378928, 2378929, 2378930, 2378935, 2378936, 2378939, and 2386027 contain the supplementary crystallographic data for this paper. The data can be obtained free of charge *via* the joint Cambridge Crystallographic Data Centre (CCDC).

Author contributions

Y. S. Shi, K. Tang, and J. C. Zhang conducted all of the reactions and data collection. J. T. Song conducted DFT calculations and experimental mechanistic studies on some aspects of characterization of the compounds, wrote the manuscript. Y. Q. Zhou contributed to crystal testing. P. Hu, B.-Q. Wang, and K.-Q. Zhao supervised and directed the project. H. F. Xiang conceptualized and directed the project, revised the manuscript. All the authors contributed to scientific discussions.

Conflicts of interest

There are no conflicts to declare.

Acknowledgements

The authors gratefully acknowledge financial support from the National Natural Science Foundation of China (No. 22405184 and 21871192), Sinopec Seed Program Project (No. 30000000-25-ZC0607-0398) and the Natural Science Foundation of Sichuan Province, China (No. 2025ZNSFSC0118). We would like to thank Prof. Dr Peng Wu and Dr Yanying Wang of Analytical & Testing Center, Sichuan University for their assistance in transient fluorescence experiments. We would also like to thank Prof. Dr Zong-Xiang Xu of Department of Chemistry, Southern University of Science and Technology for X-ray diffraction work and single-crystal analysis.

Notes and references

1 K. P. Meurer and F. Vogtle, *Top. Curr. Chem.*, 1985, **127**, 1–76.

2 (a) P. Kočovský, Š. Vyskočil and M. Smrćina, *Chem. Rev.*, 2003, **103**, 3213–3246; (b) D. Zhang, A. Martinez and J.-P. Dutasta, *Chem. Rev.*, 2017, **117**, 4900–4942.

3 (a) M. Liu, L. Zhang and T. Wang, *Chem. Rev.*, 2015, **115**, 7304–7397; (b) L.-J. Chen, H.-B. Yang and M. Shionoya, *Chem. Soc. Rev.*, 2017, **46**, 2555–2576.

4 L. Zhang, H.-X. Wang, S. Li and M. Liu, *Chem. Soc. Rev.*, 2020, **49**, 9095–9120.

5 (a) Z.-L. Gong, T.-X. Dan, J.-C. Chen, Z.-Q. Li, J. Yao and Y.-W. Zhong, *Angew. Chem. Int. Ed.*, 2024, **63**, e202402882; *Angew. Chem.*, 2024, **136**, e202402882; (b) N. Hellou, M. Srebro-Hooper, L. Favereau, F. Zinna, E. Caytan, L. Toupet, V. Dorce, M. Jean, N. Vanthuyne, J. A. G. Williams, L. Di Bari, J. Autschbach and J. Crassous, *Angew. Chem. Int. Ed.*, 2017, **56**, 8236–8239; *Angew. Chem.*, 2017, **129**, 8348–8351; (c) G. Mazzeo, S. Ghidinelli, R. Ruzziconi, M. Grandi, S. Abbate and G. Longhi, *ChemPhotoChem*, 2022, **6**, e202100222; (d) M. Ikeshita, N. Hara, Y. Imai and T. Naota, *Inorg. Chem.*, 2023, **62**, 13964–13976.

6 V. Böhmer, D. Kraft and M. Tabatabai, *J. Inclusion Phenom. Mol. Recognit. Chem.*, 1994, **19**, 17–39.

7 A. Dalla Cort, L. Mandolini, C. Pasquini and L. Schiaffino, *New J. Chem.*, 2004, **28**, 1198–1199.

8 A. Szumna, *Chem. Soc. Rev.*, 2010, **39**, 4274–4285.

9 (a) Y. Liu, Z. Ma, Z. Wang and W. Jiang, *J. Am. Chem. Soc.*, 2022, **144**, 11397–11404; (b) J.-H. Li, X.-K. Li, J. Feng, W. Yao, H. Zhang, C.-J. Lu and R.-R. Liu, *Angew. Chem. Int. Ed.*, 2024, **63**, e202319289; *Angew. Chem.*, 2024, **136**, e202319289.

10 (a) S. Tong, J.-T. Li, D.-D. Liang, Y.-E. Zhang, Q.-Y. Feng, X. Zhang, J. Zhu and M.-X. Wang, *J. Am. Chem. Soc.*, 2020, **142**, 14432–14436; (b) W. H. Powell, F. Cozzi, G. P. Moss, C. Thilgen, R. J.-R. Hwu and A. Yerin, *Pure Appl. Chem.*, 2002, **74**, 629–695; (c) E. M. G. Jamieson, F. Modicom and S. M. Goldup, *Chem. Soc. Rev.*, 2018, **47**, 5266–5311; (d) C. A. Schalley, W. Reckien, S. Peyerimhoff, B. Baytekin and F. Vögtle, *Chem.-Eur. J.*, 2004, **10**, 4777–4789.

11 (a) Z. Zhao, X. Zheng, L. Du, Y. Xiong, W. He, X. Gao, C. Li, Y. Liu, B. Xu, J. Zhang, F. Song, Y. Yu, X. Zhao, Y. Cai, X. He, R. T. K. Kwok, J. W. Y. Lam, X. Huang, D. Lee Phillips, H. Wang and B. Z. Tang, *Nat. Commun.*, 2019, **10**, 2952; (b) J.-W. Han, X.-S. Peng and H. N. C. Wong, *Natl. Sci. Rev.*, 2017, **4**, 892–916.

12 (a) M. A. Baldo, D. F. O'Brien, Y. You, A. Shoustikov, S. Sibley, M. E. Thompson and S. R. Forrest, *Nature*, 1998, **395**, 151–154; (b) E. V. Puttock, M. T. Walden and J. A. G. Williams, *Coord. Chem. Rev.*, 2018, **367**, 127–162; (c) C.-W. Chan, L.-K. Cheng and C.-M. Che, *Coord. Chem. Rev.*, 1994, **132**, 87–97; (d) X. Wu, D.-G. Chen, D. Liu, S.-H. Liu, S.-W. Shen, C.-I. Wu, G. Xie, J. Zhou, Z.-X. Huang, C.-Y. Huang, S.-J. Su, W. Zhu and P.-T. Chou, *J. Am. Chem. Soc.*, 2020, **142**, 7469–7479; (e) H. Zhang, W. Wang, C. Liu, Z. Peng, C. Du and B. Zhang, *J. Mater. Chem. C*, 2021, **9**, 9627–9636; (f) M. A. Soto, V. Carta, R. J. Andrews, M. T. Chaudhry and M. J. MacLachlan, *Angew. Chem. Int. Ed.*, 2020, **59**, 10348–10352; *Angew. Chem.*, 2020, **132**, 10434–10438; (g) Y. Wang, N. Li, L. Chu, Z. Hao, J. Chen, J. Huang, J. Yan, H. Bian, P. Duan, J. Liu and Y. Fang, *Angew. Chem. Int. Ed.*, 2024, **63**, e202403898; *Angew. Chem.*, 2024, **136**, e202403898; (h) H. Leopold, M. Tenne, A. Tronnier, S. Metz, I. Münster, G. Wagenblast and T. Strassner, *Angew. Chem. Int. Ed.*, 2016, **55**, 15779–15782; *Angew. Chem.*, 2016, **128**, 16011–16014.

13 K. M.-C. Wong and V. W.-W. Yam, *Coord. Chem. Rev.*, 2007, **251**, 2477–2488.

14 H. Xiang, J. Cheng, X. Ma, X. Zhou and J. J. Chruma, *Chem. Soc. Rev.*, 2013, **42**, 6128–6185.

15 (a) B. Li, Y. Li, M. H.-Y. Chan and V. W.-W. Yam, *J. Am. Chem. Soc.*, 2021, **143**, 21676–21684; (b) J. Gong and X. Zhang, *Coord. Chem. Rev.*, 2022, **453**, 214329; (c) G. Park, D. Y. Jeong, S. Y. Yu, J. J. Park, J. H. Kim, H. Yang and Y. You, *Angew. Chem. Int. Ed.*, 2023, **62**, e202309762; *Angew. Chem.*, 2023, **135**, e202309762.

16 L. Chassot and A. Von Zelewsky, *Helv. Chim. Acta*, 1983, **66**, 2443–2444.

17 J. R. Brandt, X. Wang, Y. Yang, A. J. Campbell and M. J. Fuchter, *J. Am. Chem. Soc.*, 2016, **138**, 9743–9746.

18 (a) T. R. Schulte, J. J. Holstein, L. Krause, R. Michel, D. Stalke, E. Sakuda, K. Umakoshi, G. Longhi, S. Abbate and G. H. Clever, *J. Am. Chem. Soc.*, 2017, **139**, 6863–6866; (b) G. Hirata, Y. Kobayashi, R. Sato, Y. Shigeta, N. Yasuda and H. Maeda, *Chem.-Eur. J.*, 2019, **25**, 8797–8804; (c) J. Song, H. Xiao, L. Fang, L. Qu, X. Zhou, Z.-X. Xu, C. Yang and H. Xiang, *J. Am. Chem. Soc.*, 2022, **144**, 2233–2244; (d) J. Song, H. Xiao, B. Zhang, L. Qu, X. Zhou, P. Hu, Z.-X. Xu and H. Xiang, *Angew. Chem. Int. Ed.*, 2023, **62**, e202302011; *Angew. Chem.*, 2023, **135**, e202302011.

19 S.-Y. Yang, Y. Chen, R. T. K. Kwok, J. W. Y. Lam and B. Z. Tang, *Chem. Soc. Rev.*, 2024, **53**, 5366–5393.

20 Y. Tu, Z. Zhao, J. W. Y. Lam and B. Z. Tang, *Natl. Sci. Rev.*, 2021, **8**, nwaa260.

21 (a) J. L.-L. Tsai, T. Zou, J. Liu, T. Chen, A. O.-Y. Chan, C. Yang, C.-N. Lok and C.-M. Che, *Chem. Sci.*, 2015, **6**, 3823–3830; (b) C. Y.-S. Chung and V. W.-W. Yam, *Chem. Sci.*, 2013, **4**, 377–387.

22 J. S. J. Tan and R. S. Paton, *Chem. Sci.*, 2019, **10**, 2285–2289.

23 D. B. Guthrie and D. P. Curran, *Org. Lett.*, 2009, **11**, 249–251.

24 E. M. Sánchez-Carnerero, A. R. Agarrabeitia, F. Moreno, B. L. Maroto, G. Muller, M. J. Ortiz and S. de la Moya, *Chem.-Eur. J.*, 2015, **21**, 13488–13500.

25 X. Zhu, Z. Wang, Y. Jia, F. Yang, Y. Zhang, S. Zhao and X. He, *J. Mater. Chem. C*, 2023, **11**, 11671–11680.

